Characterization of MRFAP1 Turnover and Interactions Downstream of the NEDD8 Pathway*[S]

Mark Larance‡, Kathryn J. Kirkwood‡, Dimitris P. Xirodimas‡§, Emma Lundberg¶, Mathias Uhlen¶, and Angus I. Lamond‡‖

The NEDD8-Cullin E3 ligase pathway plays an important role in protein homeostasis, in particular the degradation of cell cycle regulators and transcriptional control networks. To characterize NEDD8-cullin target proteins, we performed a quantitative proteomic analysis of cells treated with MLN4924, a small molecule inhibitor of the NEDD8 conjugation pathway. MRFAP1 and its interaction partner, MORF4L1, were among the most up-regulated proteins after NEDD8 inhibition in multiple human cell lines. We show that MRFAP1 has a fast turnover rate in the absence of MLN4924 and is degraded via the ubiquitin-proteasome system. The increased abundance of MRFAP1 after MLN4924 treatment results from a decreased rate of degradation. Characterization of the binding partners of both MRFAP1 and MORF4L1 revealed a complex protein-protein interaction network. MRFAP1 bound to a number of E3 ubiquitin ligases, including CUL4B, but not to components of the NuA4 complex, including MRGBP, which bound to MORF4L1. These data indicate that MRFAP1 may regulate the ability of MORF4L1 to interact with chromatin-modifying enzymes by binding to MORF4L1 in a mutually exclusive manner with MRGBP. Analysis of MRFAP1 expression in human tissues by immunostaining with a MRFAP1-specific antibody revealed that it was detectable in only a small number of tissues, in particular testis and brain. Strikingly, analysis of the seminiferous tubules of the testis showed the highest nuclear staining in the spermatogonia and much weaker staining in the spermatocytes and spermatids. MRGBP was inversely correlated with MRFAP1 expression in these cell types, consistent with an exchange of MORF4L1 interaction partners as cells progress through meiosis in the testis. These data highlight an important new arm of the NEDD8-cullin pathway. ***Molecular & Cellular Proteomics 11: 10.1074/mcp.M111.014407, 1–11, 2012.***

Quantitative proteomic analysis has become the gold standard in recent years for unbiased analysis of cellular responses to drug treatment and the analysis of protein-protein interactions. Stable isotope labeling with amino acids in cell culture (SILAC)[1] is one of the most accurate techniques for performing mass spectrometry-based quantitative proteomics experiments (1). SILAC has been used to study a wide range of cellular protein responses, including the reliable detection of specific protein interaction partners, subcellular protein localization, and changes in protein levels resulting from viral infection, drug treatments, and stress responses (2). Pulsed incorporation of amino acids containing stable isotopes was also used to measure protein turnover in nucleoli (3). Recently, detailed proteome-wide studies have used pulsed SILAC to calculate the synthesis and degradation rates of human and mouse proteins, which gives insight into protein regulation and dynamics (4, 5). In both of these studies, a subset of proteins was identified with short half-lives ($<$3 h). Among this group are two known interaction partners, *i.e.* a chromatin regulatory protein called mortality factor 4-like protein 1 (MORF4L1 or MRG15) and MORF4 family-associated protein 1 (MRFAP1).

Protein turnover plays an essential role in regulating cellular proliferation and differentiation. The ubiquitination of protein substrates mediates a large proportion of protein degradation within the cell. There are more than 600 E3 ubiquitin ligases encoded by the human genome, and of these the Cullin-based E3 ligase complexes are the most numerous and complex. The activity of Cullin E3 ligase complexes is controlled in part by their post-translational modification by the ubiquitin-like peptide NEDD8 (6, 7). NEDDylation is performed in an analogous way to ubiquitination, with NEDD8 initially binding

From the ‡Wellcome Trust Centre for Gene Regulation and Expression, College of Life Sciences, University of Dundee, Dundee, DD1 5EH, United Kingdom and the ¶Science for Life Laboratory, School of Biotechnology, KTH, Tomtebodavägen 23A, SE-171 65 Solna, Stockholm, Sweden

⌘ *Author's Choice*—Final version full access.

Received September 15, 2011, and in revised form, October 28, 2011

Published, MCP Papers in Press, October 29, 2011, DOI 10.1074/mcp.M111.014407

[1] The abbreviations used are: SILAC, stable isotope labeling with amino acids in cell culture; CUL4B, Cullin-4b; MORF4, mortality factor 4; MORF4L1, mortality factor 4-like protein 1; MRFAP1, MORF4 family-associated protein 1; MRGBP, MRG domain-binding protein; mRNA, messenger RNA; NEDD8, neural precursor cell expressed developmentally down-regulated protein 8; NuA4, nucleosome acetyltransferase of histone H4; TBST, TBS Tween 20; E1, ubiquitin-activating enzyme; E2, ubiquitin carrier protein; E3, ubiquitin-protein isopeptide ligase; MES, 4-morpholineethanesulfonic acid; IP, immunoprecipitation.

an E1 enzyme complex (APP-BP1/Uba3) (8), followed by two possible E2 enzymes for conjugation to substrates (8, 9). Several enzymes are able to catalyze deNEDDylation, at least *in vitro*, with the most well studied being the COP9 signalosome (10).

Previous studies have shown that NEDD8 conjugation to Cullins increases their ubiquitination activity and thus the degradation rate for their substrate proteins (11). A specific inhibitor of the NEDD8 E1 enzyme complex has been identified, called MLN4924 (12). MLN4924 is currently in clinical trials as an anti-cancer agent because of its ability to trigger cellular senescence, which is thought to occur after uncontrolled DNA rereplication in the S phase (12, 13). MLN4924 rapidly blocks NEDDylation of substrate proteins, including the Cullins. A recent study has reported a large scale proteomic and transcriptomic analysis of genes whose expression is altered upon blocking NEDD8 conjugation with MLN4924 in A375 human melanoma cells (14). This study identified 38 proteins as crucial to the cytotoxicity of MLN4924 in pathways such as cell cycle regulation, DNA repair, and ubiquitination (14).

The human NuA4 histone acetyltransferase complex is highly conserved from yeast to humans and is critical for the acetylation of histone H4 to regulate chromatin activity (15). Two conserved components of the NuA4 complex are MORF4L1 and MRG-binding protein (MRGBP) (15). MORF4L1 contains two domains separated by a linker region, the first being an N-terminal chromo domain that has been shown to have affinity for di- or tri-methylated histone H3 on K36 (16, 17). The second domain is the C-terminal MRG domain (MORF4-related gene domain), which has been shown to interact with MRGBP and MRFAP1 (17, 18, 20). The interaction of MORFL41 with the MRGBP protein is thought to recruit the NuA4 complex to chromatin via its chromo domain (15). The exact function of the interaction between MORF4L1 and MRFAP1 is unknown (21). However, we note that these interacting proteins were among the most rapidly turned over proteins identified in mammalian cells in the recent pulse-SILAC studies (4, 5).

In the present study, we have taken advantage of the specificity of the NEDD8 inhibitor MLN4924, combined with SILAC-based quantitative mass spectrometry methods to characterize proteins downstream of the NEDD8 pathway. Here, we report that MRFAP1, a component of the MORF4L1 complex, was stabilized dramatically by MLN4924 treatment. We present evidence based upon both protein-protein interaction studies and analysis of expression in human tissues suggesting a model in which MRFAP1 competes with MRGBP for binding to MORF4L1, thereby regulating MORF4L1 function in chromatin modification. Furthermore, examination of the human tissue expression of MRFAP1 showed that it may play a critical role in spermatogenesis, possibly by regulating the hyperacetylation of chromatin on histone H4.

EXPERIMENTAL PROCEDURES

Materials—U2OS, U138MG, Tera-1, and HaCaT cells were purchased from the American Type Culture Collection (Rockville, MD). Dulbecco's modified Eagle's medium, minimal essential medium, McCoy's 5a medium, fetal calf serum, antibiotics, NuPage gels, LDS sample buffer, MES SDS-PAGE running buffer, nitrocellulose iBlot stacks, SYPRO Ruby, Alexa Fluor 680-conjugated secondary antibodies, and CBQCA assay kit were obtained from Invitrogen. IrDye 800-conjugated secondary antibodies were obtained from Rockland Immunochemicals (Gilbertsville, PA). Histo-Clear was from National Diagnostics (Atlanta, GA). antigen unmasking solution (citric acid based) was from Vector Laboratories (Burlingame, CA). Horseradish peroxidase-conjugated secondary antibodies were from Cell Signaling Technology (Danvers, MA). Bicinchoninic acid assay reagents, Coomassie Plus (Bradford) reagent, a subcellular protein fractionation kit, detergent removal plates, 16% methanol-free paraformaldehyde, and triscarboxyethylphosphine (Bond-breaker neutral pH solution) were from Pierce. Trypsin Gold was from Promega. Sep-Pak tC18 96-well μ-elution plates were from Waters. The Pepmap C18 columns and trapping cartridges were from Dionex. Complete protease inhibitor mixture tablets and PhosStop phosphatase inhibitor tablets were from Roche Applied Science. All other materials were obtained from Sigma.

Construction of LAP1-MRFAP1 Constructs and Cell Lines—All MRFAP1 constructs were generated by gene synthesis and cloned into the pgLAP1 vector (protein sequences are provided in supplemental Fig. 3) using Gateway cloning (Invitrogen) as described previously (22).

Cell Culture—Briefly, U2OS cells were grown in Dulbecco's modified Eagle's medium supplemented with 10% FCS, 2 mM L-glutamine, 100 units/liter penicillin, and 100 μg/liter streptomycin at 37 °C in 10% CO_2 and passaged at ~80% confluence. U2OS cells expressing LAP1-tagged proteins were grown in the same medium as U2OS but with the addition of 150 μg/ml hygromycin B and 15 μg/ml blasticidine HCl. HaCaT cells were cultured in Dulbecco's modified Eagle's medium supplemented with 10% FCS, 100 units/liter penicillin, and 100 μg/liter streptomycin at 37 °C in 10% CO_2 and passaged at ~80% confluence. Tera-1 cells were cultured in McCoy's 5a medium supplemented with 20% FCS, 100 units/liter penicillin, and 100 μg/liter streptomycin at 37 °C in 10% CO_2 and passaged at ~80% confluence. U138MG cells were cultured in minimal essential medium supplemented with 10% FCS, 100 units/liter penicillin, and 100 μg/liter streptomycin at 37 °C in 10% CO_2, and passaged at ~80% confluence. For SILAC labeling of U2OS cells, arginine- and lysine-free Dulbecco's modified Eagle's medium was used and supplemented with stable isotope-labeled arginine and lysine in addition to dialyzed FCS as described previously (23).

Subcellular Fractionation of U2OS Cells—For the initial SILAC screen U2OS cells were treated with either DMSO or MLN4924, combined in a 1:1 ratio of cells and fractionated using differential centrifugation and sucrose cushions as described previously to obtain crude cytoplasmic, nucleoplasmic, and nucleolar fractions (24). These three fractions were then chloroform methanol-precipitated (25) and further separated by molecular weight using denaturing size exclusion chromatography prior to digestion and LC-MS/MS analysis.

A Pierce subcellular protein fractionation kit was used to fractionate U2OS cells according to the manufacturer's instructions. Each fraction was chloroform methanol-precipitated prior to analysis by SDS-PAGE and immunoblotting.

SDS-PAGE and Immunoblotting—Equal amounts of protein were loaded for SDS-PAGE of each sample with 10 μg/lane, except for immunoprecipitation eluates where 10% of the elution volume was loaded. SDS-PAGE was performed using on 4–12% (w/v) Bis-Tris NuPage gels using MES running buffer according to manufacturer's

instructions but with the addition of 25 mM triscarboxyethylphosphine, in the LDS sample buffer. Equal amounts of protein were loaded with a maximum of 10 μg/lane. SYPRO Ruby staining was performed as per manufacturer's instructions (Invitrogen). For mass spectrometric identification SYPRO Ruby staining was performed as per the manufacturer's instructions. For Western blotting, separated proteins were electrophoretically transferred to an iBlot nitrocellulose membrane, blocked with 3% nonfat skim milk in 0.1% Tween 20 in TBS (TBST), and incubated with primary antibody in 5% BSA in TBST overnight at 4 °C. After incubation, the membranes were washed three times in TBST and incubated with horseradish peroxidase-labeled or Alexa fluor 680/IrDye 800-labeled secondary antibodies in 3% nonfat skim milk in TBST. Proteins were visualized using Immobilon chemiluminescent substrate (Millipore) and imaged with a cooled CCD camera (Fuji) for horseradish peroxidase-labeled secondary antibodies or a Licor Odyssey imager for Alexa Fluor 680/IrDye 800-labeled secondary antibodies.

Denaturing Gel Filtration Chromatography, Trypsin Digestion, and Peptide Clean-up—Using a Dionex Ultimate 3000 HPLC system, fractions resuspended in 4% SDS, 100 mM NaCl, 25 mM triscarboxyethylphosphine, 50 mM *N*-ethylmaleimide, 10 mM Na PO_4, pH 6.0, were heated to 65 °C for 10 min and then filtered through a 0.45-μm filter. The samples were injected (20 μl/injection for 100 μg of protein) onto a mAbPacSEC column (Dionex) equilibrated with 0.2% SDS, 100 mM NaCl, 10 mM Na PO_4, pH 6.0. The flow rate was 0.2 ml min^{-1}, and 16 fractions of 100 μl were collected using a low protein binding 96-deep well plate (Eppendorf). Triethylamine bicarbonate (1 M, pH 8.0) was added to each fraction to adjust the pH to 8.0, and trypsin diluted in 0.1 M triethylamine bicarbonate was added at a ratio of 1:50 with incubation for 18 h at 37 °C. SDS was removed from each fraction using detergent removal resin in 96-well plates as described previously (26). For peptide desalting, trifluoroacetic acid was added to 1% (v/v) final concentration, and peptides were purified using a Sep-Pak tC18 96-well μ-elution plate. The peptides were eluted in 200 μl of 50% (v/v) acetonitrile and dried with a SpeediVac prior to resuspension in 5% (v/v) formic acid. Peptide concentrations were determined using the CBQCA assay after 25-fold dilution of peptide samples in 0.1 M borate buffer, pH 9.3.

LC-MS/MS and Maxquant Analysis—Using a Dionex Ultimate 3000 nanoHPLC system, 1 μg of peptides in 5% (v/v) formic acid were injected onto an Acclaim PepMap C18 nano-trap column (Dionex). After washing with 2% (v/v) acetonitrile, 0.1% (v/v) formic acid peptides were resolved on a 150-mm × 75-μm Acclaim PepMap C18 reverse phase analytical column over a 100-min organic gradient with a flow rate of 300 nl min^{-1}. The peptides were ionized by nano-electrospray ionization at 1.2 kV using a fused silica emitter with an internal diameter of 5 μm (New Objective). Tandem mass spectrometry analysis was carried out on a LTQ-Velos Orbitrap mass spectrometer Thermo Scientific. The data-dependent acquisition method used was the FT10 protocol as described previously (27). The data were processed, searched, and quantified using the Maxquant software package version 1.2.0.18 as described previously (28), using the default settings and employing the human Uniprot database (June 7, 2011) containing 109,824 entries. The settings used for the Maxquant analysis were: two failed cleavages were allowed; fixed modification was *N*-ethylmaleimide on cysteine; enzymes were trypsin (K/R not before P); variable modifications included in the analysis were methionine oxidation, deamidation of glutamine or asparagine, N-terminal pyroglutamic acid formation, and protein N-terminal acetylation. A mass tolerance of 7 ppm was used for precursor ions, and a tolerance of 0.5 Da was used for fragment ions. Using the default Maxquant settings, a maximum false positive rate of 1% was allowed for both peptide and protein identification. This cut-off was used for accepting individual spectra, as well as whole proteins in the Maxquant output. This threshold has previously been shown to be a rigorous method for identifying true positive matches (28). All of the replicates indicated are biological replicates. Protein quantitation data were always derived from a minimum of two or more peptides/protein.

GFP-IP from SILAC-labeled U2OS Cells—The cells for each condition were harvested separately by trypsinization, washed in PBS, and lysed in IP buffer (1% Nonidet P-40, 50 mM Tris-Cl, pH 7.4, 10% glycerol, 150 mM NaCl, Roche Applied Science Complete protease inhibitor mixture, PhosStop, 50 mM *N*-ethylmaleimide). The lysate was centrifuged for 10 min at 17,000 × *g* at 4 °C. Equal protein amounts of each sample were then incubated with GFP-trap agarose beads from ChromoTek (Martinsried, Germany) that had been washed once in IP buffer (40 μl of 50% GFP-trap bead slurry per IP) and were incubated for 2 h at 4 °C. The beads were then washed three times with IP buffer by centrifugation at 2000 × *g* for 2 min at 4 °C. SILAC mixing was performed in the first wash. The beads were resuspended in 200 μl of PBS and transferred to a spin column (Pierce) and centrifuged dry at 500 *g* for 1 min. LDS sample buffer that had been preheated to 65 °C was then added and incubated at 65 °C for 5 min. The eluate was collected by centrifugation at 500 × *g* for 1 min at room temperature.

Immunofluorescence Microscopy—The cells were cultured on glass coverslips as described above. All of the subsequent steps are at 25 °C. The cells were then fixed with 3% paraformaldehyde in PBS. Fixed cells were washed with PBS, and free aldehyde groups were quenched with 50 mM glycine in PBS. The cells were then permeabilized using 1% Triton X-100 for 10 min followed by washing in PBS. Coverslips were processed for immunolabeling by blocking with 5% BSA in TBST. Primary antibodies were incubated on coverslips for 1 h in 5% BSA in TBST. The coverslips were washed by dipping 10 times into 500 ml of PBS. Primary antibodies were detected with Alexa Fluor 488- or Alex Fluor 594-conjugated secondary antibodies that were incubated on coverslips for 30 min in 5% BSA in TBST.

For paraffin-embedded paraformaldehyde-fixed mouse tissue sections (7 μm thick), deparaffinization was performed using Histo-Clear according to the manufacturer's instructions. Citrate-based unmasking solution was used for antigen retrieval according to manufacturer's instructions. The cells were permeabilized using 1% Triton X-100 for 15 min followed by washing in PBS. Four 15-min incubations with 1% sodium borohydride were used for autofluorescence reduction. The tissues were processed for immunolabeling by blocking with 5% donkey serum in PBS with 0.3% Triton X-100. Primary antibodies were incubated overnight in 5% donkey serum in PBS with 0.3% Triton X-100 at 4 °C. Primary antibodies were detected with Alexa Fluor 488- or Alex Fluor 594-conjugated secondary antibodies that were incubated for 1 h in 5% donkey serum in PBS with 0.3% Triton X-100 at 25 °C in the dark. Optical sections were analyzed by confocal microscopy on a Leica SP2 AOBS inverted microscope. Images were generated by the maximum projection of a z-stack taken from the top to the bottom of the cell monolayer. Contrast was adjusted for all images with the same settings.

RESULTS

Identification of Proteins Downstream of NEDD8-Cullin Pathway—Using a high specificity inhibitor of the NEDD8 E1 enzyme (MLN4924), we have interrogated the NEDD8 pathway in U2OS cells. Given that NEDD8 conjugation to Cullins is known to regulate their E3 ubiquitin ligase activity, we chose to identify those proteins whose expression increased after NEDD8 inhibition and therefore may be regulated downstream of the Cullins. We have used SILAC-based quantitative proteomics to perform a differential screen comparing the

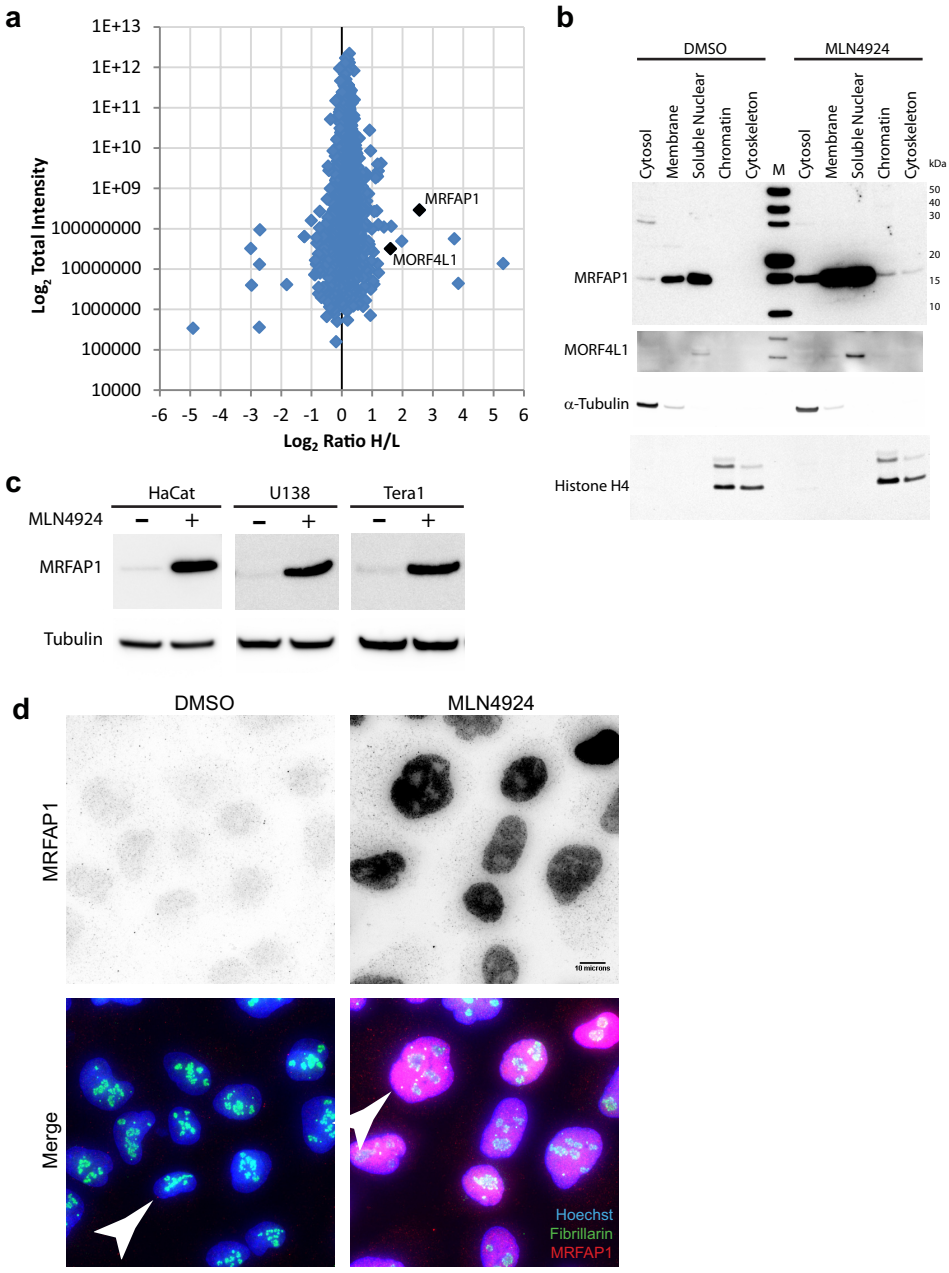

FIG. 1. **MRFAP1 and MORF4L1 are up-regulated in response to NEDD8 inhibition.** *a*, SILAC analysis of U2OS cells following NEDD8 inhibition. The abundance of ~2,500 proteins is indicated on the *y axis* using a $\log_2$ scale. The abundance of each protein indicated by the position of the dot on the *y axis* was determined by summing up all individual light and heavy peptide intensities detected for each protein. The relative fold decrease or increase is shown using the $\log_2$ ratio (heavy/light) on the *x axis*, with 1 μM MLN4924 treatment for 18 h (heavy) over DMSO only (light) ($n = 2$). *b*, immunoblotting of subcellular fractionation from U2OS cells treated with 1 μM MLN4924 treatment for 18 h or DMSO only ($n = 3$). *c*, immunoblotting of total cell lysates from the indicated cell types treated with 1 μM MLN4924 treatment for 18 h or DMSO only ($n = 2$). *d*, immunofluorescence microscopy of endogenous MRFAP1 in U2OS cells treated with 1 μM MLN4924 treatment for 18 h or DMSO only. The *white arrowheads* indicate change in nuclear size after MLN4924 treatment ($n = 3$). The *scale bar* indicates 10 μm.

relative abundance of proteins either in control, DMSO-treated U2OS cells or in U2OS cells treated for 18 h with 1 μM MLN4924 grown in medium containing either light (R0K0) or heavy (R10K8) stable isotope-labeled amino acids, respectively. Protein extracts from both the control and MLN4924-treated cells were mixed, fractionated, digested with trypsin into peptides, and analyzed by mass spectrometry on a LTQ Velos as described under "Experimental Procedures." Peptides were identified, and SILAC ratios were quantitated using MaxQuant, which showed that of >2,500 protein groups detected, 32 protein groups increase more than 2-fold in relative abundance after 18 h of MLN4924 treatment (Fig. 1*a* and

supplemental Table 1). Among these up-regulated proteins, MRFAP1 and MORF4L1 stood out from the top six most up-regulated proteins because they had been previously shown to be interaction partners (18) and to have fast turnover rates (4, 5). These two proteins were therefore selected for further analysis.

We confirmed the MS identification data using subcellular fractionation and protein blotting with antibodies specific for MRFAP1 and MORF4L1, which also showed that MRFAP1 and MORF4L1 are predominantly soluble nuclear proteins whose abundance increases following treatment of cells with MLN4924 (Fig. 1*b*). To determine whether the increase in the abundance of MRFAP1 in response to NEDD8 inhibition was conserved across different cell types, we also treated HaCaT (keratinocytes), U138MG (gliobastoma), and Tera-1 (pluripotent testicular teratoma) cells with MLN4924. Immunoblotting of total cell lysates from each of these cell types confirmed up-regulation of MRFAP1 levels in each case (Fig. 1*c*). To ensure that the antibody was specifically recognizing MRFAP1 and not other proteins in the extracts, we utilized siRNA knockdown of MRFAP1 in several cell lines, followed by both immunoblotting and indirect immunofluorescence microscopy (supplemental Fig. 1). In each case a major band at ~15 kDa, the predicted size for MRFAP1, was detected that was reduced after siRNA treatment with oligonucleotides specific for MRFAP1. These data showed that the antibody recognizes MRFAP1 specifically in multiple cell lines and would be useful for further analysis of the protein. To confirm the subcellular localization of MRFAP1, indirect immunofluorescence microscopy was performed on U2OS cells either with or without MLN4924 treatment. This showed MRFAP1 to have a nucleoplasmic localization that was increased in abundance after NEDD8 inhibition (Fig. 1*d*). A marked increase in nuclear size was also observed (Fig. 1*d*, *arrowheads*) and would be consistent with DNA rereplication, which is a known consequence of MLN4924 treatment (12).

MRFAP1 Is Stabilized by NEDD8 Inhibition and Co-expression of MORF4L1—To determine how MRFAP1 protein abundance was increased after NEDD8 inhibition, we tested whether the degradation of the protein was altered either with or without overnight MLN4924 treatment. A cycloheximide time course after overnight incubation of U2OS cells with either 1 μM MLN4924 or DMSO control treatment showed, as expected, an increase in MRFAP1 protein abundance upon NEDD8 inhibition, as well as a decrease in the rate of MRFAP1 degradation (Fig. 2*a*). Strikingly, analysis of DMSO-treated control cells showed MRFAP1 to have a very fast turnover rate, with almost no protein detected after 2 h of cycloheximide treatment. To confirm this result, we examined the turnover of LAP1-tagged, wild type MRFAP1 (supplemental Fig. 3*a*) expressed in an inducible stable U2OS cell line as described previously (22). Using an 8-h time course of cycloheximide treatment, we showed that the exogenous MRFAP1 had very similar degradation kinetics to endogenous

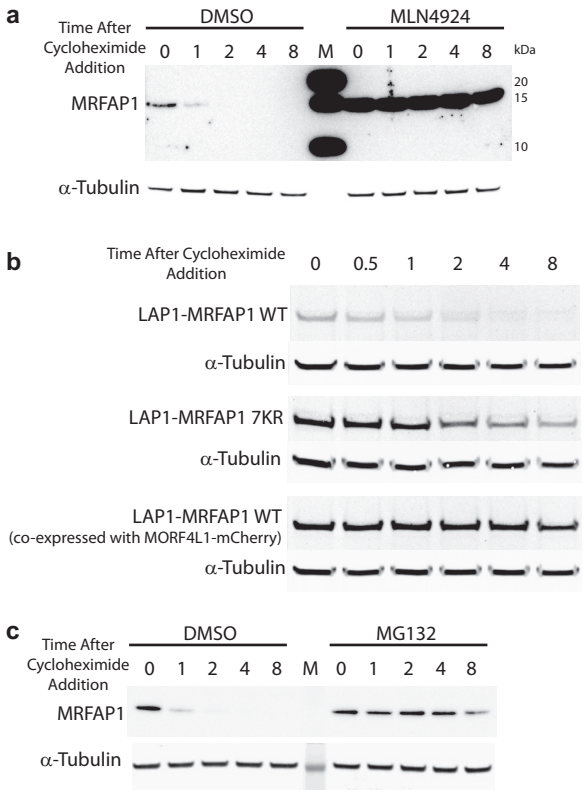

FIG. 2. **MRFAP1 is stabilized by NEDD8 inhibition.** *a*, immunoblotting of total cell lysates from U2OS cells treated with 1 μM MLN4924 for 18 h or DMSO only. A time course of cycloheximide treatment followed to examine protein degradation ($n = 3$). *b*, immunoblotting of total cell lysates from either LAP1-MRFAP1 wild type, LAP1-MRFAP1 7KR, or LAP1-MRFAP1-P2A-MORF4L1-mCherry after a time course of cycloheximide treatment to examine protein degradation ($n = 2$). *c*, immunoblotting of total cell lysates from U2OS cells treated with 10 μM MG132 or DMSO only. A time course of cycloheximide treatment was used to examine protein degradation. MG132 and cycloheximide were added at the same time for each time point ($n = 3$).

MRFAP1 (Fig. 2*b*). To determine whether this degradation was mediated via ubiquitin conjugation, we constructed a LAP1-tagged MRFAP1 mutant that was not competent for ubiquitin conjugation (7KR), which was expressed in a second inducible stable U2OS cell line just as for the wild type protein (Fig. 2*b*). In the 7KR mutant, all seven lysine residues in the MRFAP1 protein have been mutated to arginines (supplemental Fig. 3*b*), thereby preventing modification by ubiquitin, which must be linked to lysine residues. This fusion protein can, however, still be ubiquitinated within the LAP1 tag, which contains lysine residues (22). Regardless, the MRFAP1 7KR mutant was more stable than the wild type protein (Fig. 2*b*). To test whether it was the co-expression of MRFAP1 and MORF4L1 after MLN4924 treatment that helped stabilize each protein, we generated a third inducible stable cell line expressing each protein at close to equimolar levels. This cell line was generated using a new construct consisting of LAP1-tagged wild type MRFAP1 followed by a picornoviral ribo-

some skipping sequence (29) and then MORF4L1-mCherry (supplemental Fig. 3*c*). The exogenous LAP1-MRFAP1 in these cells showed similar increased stability in the presence of equimolar amounts of MORFL41 to that of endogenous MRFAP1 from cells treated with MLN4924 (Fig. 2*b*). To determine whether endogenous MRFAP1 degradation was mediated via the proteasome, we exposed U2OS cells to a cycloheximide time course with either 10 μM MG132 or DMSO control treatment. This showed, as expected, an increase in MRFAP1 protein abundance upon proteasome inhibition as well as a decrease in the rate of MRFAP1 degradation (Fig. 2*c*).

MRFAP1 Interacts with E3 Ubiquitin Ligases—Next we investigated which proteins may be controlling MRFAP1 and MORF4L1 turnover. To do this, we constructed inducible U2OS stable cell lines that express either wild type LAP1-MRFAP1 or wild type LAP1-MORF4L1 and used them to perform SILAC-based quantitation of the interaction partners for each of these proteins (22). In these triple SILAC experiments, we compared GFP-based immunoprecipitates from uninduced cells (light), doxycycline-induced (medium), and doxycycline-induced cells with simultaneous MLN4924 treatment (heavy). This experimental design allowed discrimination between strong interactors and contaminant proteins for each of the three conditions. Analysis of the LAP1-MRFAP1 immunoprecipitates revealed strong binding to previously identified interaction partners of MRFAP1, including MORF4L1 and MORF4L2, which were enriched in MLN4924-treated cells because of their increased abundance after NEDD8 inhibition (Fig. 3*a*). A number of ubiquitination-related proteins were also identified, as well as ubiquitin itself, including the HECT domain-containing E3 ligases UBR5 (EDD) and HUWE1, Cullin-4A/B, and one of its substrate-binding proteins VprBP, as well as the deubiquitination enzyme OTUB1. In addition, MRFAP1 showed interactions with coronin-1c, a WD40-repeat containing protein, which has previously been associated with F-actin binding but may have other roles with regard to MRFAP1 regulation. We were unable to detect any chromatin modification/remodeling enzymes in our MRFAP1 immunoprecipitates, which may indicate that MRFAP1, which binds to MORF4L1 via its MRG domain (20), blocks the MORF4L1 interaction with these complexes. Curiously, we consistently observed increased background binding of proteins from cells treated with MLN4924 as seen in Fig. 3*a* by the cloud of background binders offset from (0, 0). This phenomenon may relate to the effect of the drug on cellular architecture/cytoskeleton.

After comparing the SILAC ratios for each of these interactors, it was clear that VprBP and Cullin-4A/B only interacted strongly with MRFAP1 following MLN4924 treatment. This could be the result of an inactive cullin being unable to dissociate from its substrate because of an inability to carry out ubiquitination. To verify these data, we again immunoprecipitated LAP1-MRFAP1 from extracts of cells treated with MLN4924, separated the proteins by SDS-PAGE, and immunoblotted with antibodies specific for Cul4b, VprBP, and Cul4a. These data showed that Cul4b, but not Cul4a, was co-immunoprecipitated with MRFAP1 and confirmed our mass spectrometry quantitation, because the association of MRFAP1 with Cul4b was almost undetectable in untreated cells but was clearly seen from cells treated with either MLN4924 or MG132 (Fig. 3*b*). The interaction between

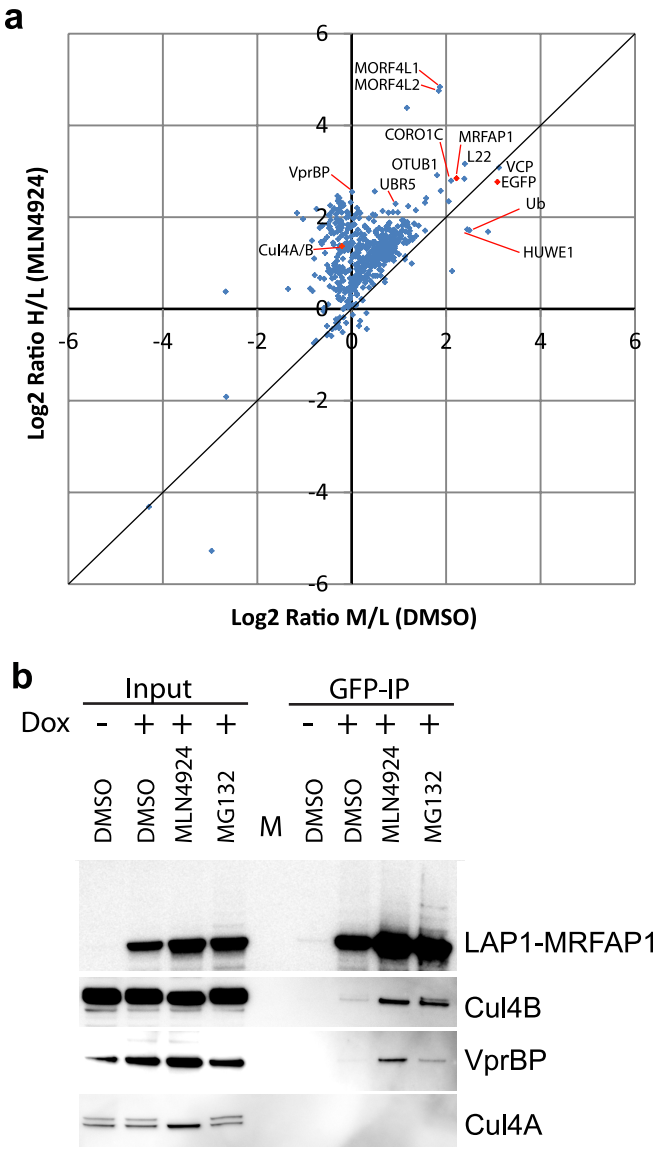

FIG. 3. **MRFAP1 interacts with ubiquitin E3 ligases.** *a*, SILAC GFP-IP analysis of U2OS cells stably expressing inducible LAP1-MRFAP1 wild type. GFP immunoprecipitates from uninduced (light), doxycycline-induced (medium), and doxycycline-induced cells with simultaneous MLN4924 treatment (heavy) were mixed and analyzed together by LC-MS/MS. The $\log_2$ ratio (medium/light) is indicated on the *x axis*. The $\log_2$ ratio (heavy/light) is indicated on the *y axis*. High ratios indicate high abundance of interaction compared with control. Proteins of interest are indicated ($n = 2$). *b*, immunoblotting of GFP-immunoprecipitated LAP1-MRFAP1. The cells were treated with 1 μM MLN4924 for 18 h or DMSO only ($n = 3$).

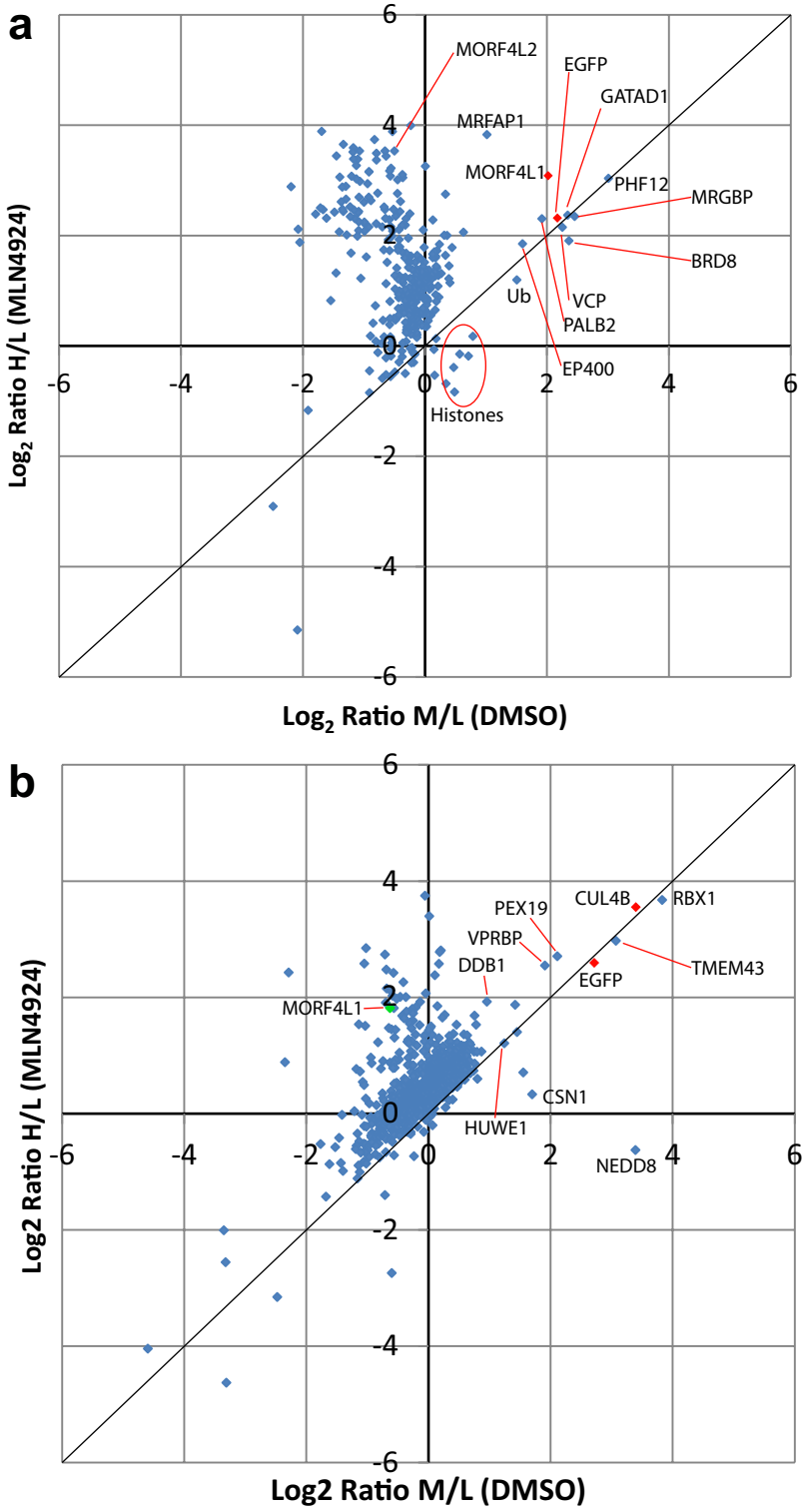

FIG. 4. **MRFAP1 is part of a complex protein-protein interaction network.** *a*, SILAC GFP-IP analysis of U2OS cells stably expressing inducible LAP1-MORF4L1. *b*, SILAC GFP-IP analysis of U2OS cells stably expressing inducible LAP1-CUL4B. GFP immunoprecipitates from uninduced (light), doxycycline-induced (medium), and doxycycline induced cells with simultaneous MLN4924 treatment (heavy) were mixed and analyzed together by LC-MS/MS. The $\log_2$ ratio (medium/light) is indicated on the *x axis*. The $\log_2$ ratio (heavy/light) is indicated on the *y axis*. High ratios indicate high abundance of interaction compared with control. Proteins of interest are indicated ($n = 1$).

MRFAP1 and VprBP was also confirmed and showed the strongest binding with MLN4924 treatment and weaker binding with MG132 treatment.

Analysis of the LAP1-MORF4L1 immunoprecipitates revealed strong binding to previously identified interaction partners of MORF4L1, including MRFAP1 and MRGBP, both of which bind to MORFL4 through its MRG domain (Fig. 4*a*). We observed strong binding to a number of other components of the NuA4 histone acetylation complex in addition to MRGBP, including BRD8 and EP400. Components of other chromatin-

modifying complexes were also seen, including GATAD1, a component of the JARID1A histone demethylase complex and PHF12, a component of the Sin3a histone deacetylase complex. Weaker interaction of MORFL41 with all of the core histones was also seen in control cells, but this was decreased after MLN4924 treatment. The recently identified MORF4L1-binding, DNA damage response protein PALB2 (FANCN) was also observed in our immunoprecipitates (30, 31). These data provide an overview of the variety of MORF4L1-containing complexes within U2OS cells and demonstrate our ability to observe several low abundance protein complexes.

To further clarify the role of Cul4B in the regulation of MRFAP1, we also carried out immunoprecipitation experiments to detect LAP1-CUL4B-interacting partner proteins in extracts from cells either with or without MLN4924 treatment (Fig. 4*b*). These data demonstrated how effective NEDD8 deconjugation was for Cul4b after MLN4924 treatment. Thus, we can clearly see NEDD8 association with Cul4b in untreated cells, as well as association with components of the deNEDDylating COP9 signalosome, such as CSN1 (10), as indicated by the high positive M/L ratio observed for these proteins. However, these interactions are largely abolished in MLN4924-treated cells as indicated by the negative H/L ratio observed for these proteins. We also observed interaction of Cul4b with the substrate-binding protein VprBP, which we also observed interacting with MRFAP1. However, MRFAP1 itself was not observed. MORF4L1 was observed interacting with Cul4b in MLN4924-treated cells, again indicating that Cul4b has an increased affinity for the MRFAP1-MORF4L1 complex after NEDD8 inhibition. TMEM43, which is a component of the inner nuclear membrane (32), showed a strong interaction that may be related to the nuclear localization of Cul4b in U2OS cells (Human Protein Atlas) (33). RBX1 and DDB1 are previously known components of Cul4b-containing protein complexes (34).

MRFAP1 Is Inversely Correlated with MRGBP Expression in Testis—Next we used a complementary microscopy-based strategy to investigate the expression pattern and associations of the interacting proteins identified above. Using the antibody specific for MRFAP1, which we previously validated by siRNA knockdown in a variety of cell types, we examined the tissue microarrays developed for the Human Protein Atlas project (33) to determine the expression pattern and subcellular localization of MRFAP1 in normal and cancerous human tissue (supplemental Tables 2 and 3). This analysis revealed that MRFAP1 had moderate nuclear expression in the spermatogonia of the testis, strong nuclear or cytoplasmic expression in ciliated epithelia, and strong cytoplasmic expression in neurons (Fig. 5*a*, nuclear staining indicated by *arrowheads*), whereas most other tissues had weak or negative staining (supplemental Table 2). The expression of MRFAP1 in spermatogonia may indicate that the protein plays some role in spermatogenesis and the initial stages of meiosis (supplemental Fig. 4).

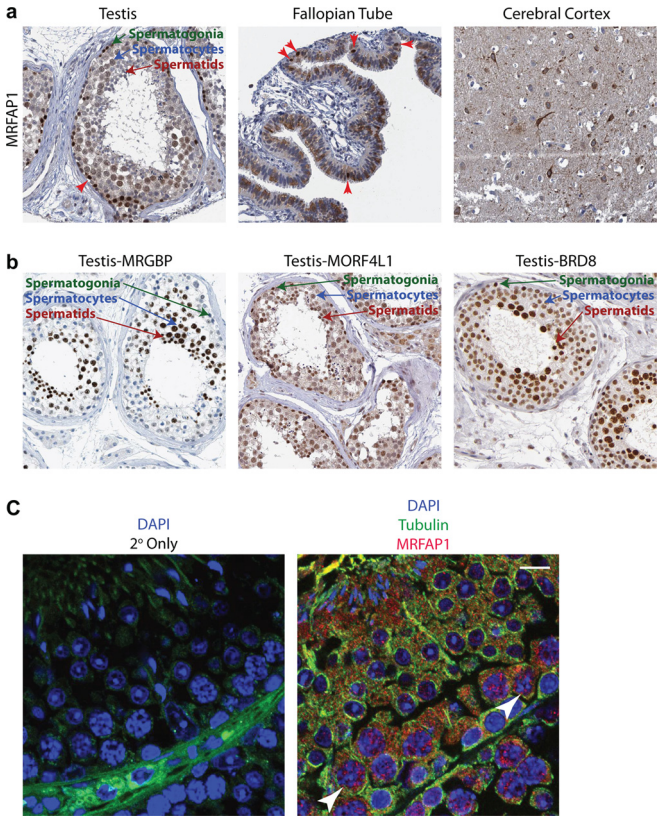

FIG. 5. **Human normal tissue expression pattern of MRFAP1.** *a*, immunohistochemistry imaging of endogenous MRFAP1 in selected tissues. The *brown color* indicates staining ($n = 3$). The *red arrows* indicate nuclear staining in spermatogonia of testis and ciliated epithelial cells of the fallopian tube. *b*, immunohistochemistry imaging of endogenous protein as indicated in testis tissue. The *brown color* indicates staining ($n = 3$). *c*, immunofluorescence microscopy of endogenous MRFAP1 in murine testis tissue ($n = 3$). The *red arrows* indicate nuclear staining in spermatogonia of testis. The *scale bar* indicates 10 μm.

To determine how the expression patterns of MORFL41, MRGBP, and BRD8 compared with that of MRFAP1, we examined the Human Protein Atlas testis tissue staining data (33), which utilized antibodies recognizing each of these proteins. This showed that MORF4L1 was detected at all cell stages of spermatogenesis, but that MRGBP and BRD8, two components of the NuA4 histone acetyltransferase complex, were highly enriched in spermatocytes and spermatids (Fig. 5*b*; Ref. 33; also see supplemental Fig. 4 for a description of spermatogenesis in the testis). Strikingly, when MRGBP expression in all tissues was examined, testis showed the strongest expression, and most other tissues were negative (33). In cancer tissues, MRFAP1 showed a very similar expression pattern to normal tissues, with the highest expression in glioblastoma and testicular cancer (supplemental Table 3). However, the MRGBP protein was largely undetectable in testicular cancer, in stark contrast to its expression in normal tissues. To confirm the subcellular localization of MRFAP1 in normal testis, we performed indirect immunoflu-

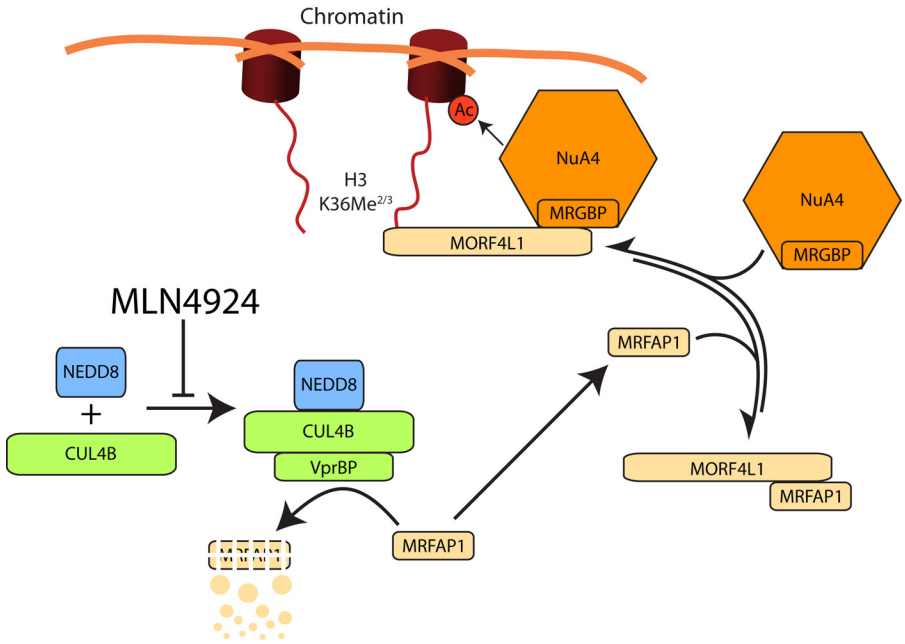

FIG. 6. **Model for the regulation of MRFAP1 by the NEDD8 pathway.** The NuA4 histone acetyltransferase complex is recruited to chromatin via the binding of MORF4L1 to tri/di-methylated lysine 36 on histone H3. Cells treated with MLN4924 have a defect in NEDD8 conjugation; therefore Cul4b would be less active in MRFAP1 degradation. An increase in free MRFAP1 protein displaces MRGBP from MORF4L1 and creates a stable MORF4L1-MRFAP1 complex.

orescence confocal microscopy on mouse testis sections (Fig. 5*c*). This analysis confirmed the nuclear localization of MRFAP1 in spermatogonia (Fig. 5*c*, *white arrowheads*). We conclude that in human seminiferous tubules of the testis, the MORF4L1 protein is expressed in all cells, but with a largely mutually exclusive co-expression of the alternate interacting proteins MRFAP1 and MRGBP.

DISCUSSION

In the present study, we have used SILAC-based quantitative mass spectrometry to characterize several nuclear proteins regulated by the NEDD8 pathway. We have identified MRFAP1 and MORF4L1 as being up-regulated in U2OS cells in response to inhibition of NEDD8 conjugation by treatment of cells with the inhibitor MLN4924. The up-regulation of MRFAP1 is mediated by an increase in the stability of the MRFAP1 protein after MLN4924 treatment. This stabilization could be enhanced because of the formation of a stable complex between MRFAP1 and MORF4L1. We further interrogated the protein-protein interaction network formed by these proteins and identified the E3 ubiquitin ligase Cul4b complex as binding to MRFAP1. This provides a putative mechanism to link the NEDD8-regulated Cul4b protein and stabilization of MRFAP1 (Fig. 6). We also saw that MRFAP1 and MRGBP could not be co-immunoprecipitated and therefore may bind in a mutually exclusive manner to MORFL41. We infer that MRFAP1 could therefore act as a regulator of MORF4L1 activity by changing its binding partners.

The proteomic analysis we present here highlighted only a subset of proteins whose expression was up-regulated by 18 h of MLN4924 treatment. The short period of NEDD8 conjugation inhibition used in this study may favor the detection of proteins that are rapidly degraded, downstream of the NEDD8-cullin E3 ubiquitin ligase pathways. A recent study that examined in detail the transcriptional and proteome response to MLN4924 treatment in human A375 melanoma cells reported a larger number of proteins whose abundance was altered (14). This may reflect differences in the cell types studied and/or experimental conditions used. Regardless, Liao *et al.* (14) also observe the increased abundance of MRFAP1 and MORF4L1 in human A375 melanoma cells after MLN4924 treatment, which adds further evidence to the universal response of cells to up-regulate these proteins after NEDD8 conjugation inhibition.

Analysis of the human tissue expression pattern of MRFAP1 showed it to be expressed in only a few cell types, including spermatogonia, ciliated epithelial cells, and neurons. Closer examination of the testis expression pattern for MRFAP1 and MRGBP indicated an anti-correlated pattern, suggesting that recruitment of NuA4 histone acetyltransferase activity to chromatin via MORFL41 might be important for later stages of spermatogenesis. This is because only the cells in later stages of spermatogenesis showed co-expression of MRGBP and MORF4L1 but not MRFAP1. The MORF4L1-MRGBP modification complex could be inhibited in spermatogonia because of high MRFAP1 expression, which we suggest competes with MRGBP for binding to MORF4L1. We propose that this may block the hyperacetylation pathway in spermatogonia to maintain a germ stem cell population.

Previous studies have shown in a number of animals, including rats and mice, that hyperacetylation of histone H4 is critical for spermatogenesis (35, 36). These studies showed that hyperacetylation of histone H4 leads to chromatin decondensation, which is thought to allow for histone replacement by protamines and thereby facilitate the extensive chromatin compaction needed in the small sperm nu-

cleus (supplemental Fig. 4). We propose that the NuA4 histone acetyltransferase complex, which contains MRGBP and BRD8, plays a critical role in spermatogenesis by mediating the hyperacetylation of histone H4. One of the other MORF4L1-interacting proteins we observed was EP400, which as part of the human NuA4 complex may also play a role in the exchange of histone H2A for histone H2A.Z during spermatogenesis (37).

The MRFAP1 protein is highly conserved and only present in mammals, consistent with it playing a specific role in the regulation of MORF4L1 protein complexes (supplemental Fig. 2). MRFAP1 may thus be expressed in spermatogonia to maintain normal levels of histone modification by negatively regulating recruitment of the NuA4 complex to chromatin (Fig. 6).

Analysis of the MRFAP1 domain structure shows that it is a relatively simple, modular protein, with an N-terminal MRG-binding domain followed by a flexible linker region containing a number of glycine residues and a C-terminal coiled coil region that could mediate homodimerization of the MRFAP1 protein (38–40). The dimerization capability of MRFAP1 could reflect the fact that the MRG domain of MORF4L1 is a dimer, the structure of which has been solved by x-ray crystallography (20). We propose that a homodimer of MRFAP1 may bind the homodimer of MORF4L1, forming a high affinity interaction between the two dimers. The abundance of the MORF4L1-MRFAP1 complex, compared with the MORF4L1-MRGBP complex, would then be mediated, at least in part, by the probability of an encounter between each of these proteins and therefore is related to the abundance and localization of each protein (19).

Our studies here using quantitative proteomics analyses have revealed new evidence for the functional role of NEDD8 modification in controlling gene expression during cell differentiation in mammals. This has opened up new avenues to investigate mechanisms regulating histone acetylation and its link with spermatogenesis. In view of the tissue specificity of MRFAP1 and MRGBP expression, it is possible that these proteins regulate the hyperacetylation of histone H4 during spermatogenesis via a pathway dependent upon binding stoichiometry. In the context of cancer, this pathway may be involved by subtly altering the histone modifications of chromatin, thereby altering gene expression to favor cancer cell proliferation. Our data provide evidence for a combinatorial mechanism affecting cell-specific regulation of chromatin modification that involves changing the balance between MRFAP1-MORF4L1-MRGBP interactions. In future, it will be of interest to characterize further the impact of this pathway in disease states, such as cancer, that are influenced by alterations in histone acetylation and related modifications.

* This work was supported by Wellcome Trust Grants 083524/Z/07/Z, 073980/Z/03/Z, 08136/Z/03/Z, and 0909444/Z/09/Z; EU FP7 Prospects Network Grant HEALTH-F4–2008-201648; and European Union FP7 Epigenesis Network Grant HEALTH-F4-2010-257082. The Human Protein Atlas project was funded by the Knut and Alice Wallenberg Foundation. The costs of publication of this article were defrayed in part by the payment of page charges. This article must therefore be hereby marked "*advertisement*" in accordance with 18 U.S.C. Section 1734 solely to indicate this fact.

S This article contains supplemental Tables 1–3 and Figs. 1–4.

§ Association for International Cancer Research Fellow. Present address: Universités Montpellier 2 et 1, Centre de Recherche de Biochimie Macromoléculaire, CNRS UMR 5237, Montpellier, France.

‖ Wellcome Trust Principal Research Fellow. To whom correspondence should be addressed: Wellcome Trust Centre for Gene Regulation and Expression, College of Life Sciences, University of Dundee, Dow St., Dundee, UK. Tel.: 44-01382385473; Fax: 44-01382385695.

REFERENCES

1. Ong, S. E., Blagoev, B., Kratchmarova, I., Kristensen, D. B., Steen, H., Pandey, A., and Mann, M. (2002) Stable isotope labeling by amino acids in cell culture, SILAC, as a simple and accurate approach to expression proteomics. *Mol. Cell. Proteomics* **1,** 376–386
2. Cox, J., and Mann, M. (2011) Quantitative, high-resolution proteomics for data-driven systems biology. *Annu. Rev. Biochem.* **80,** 273–299
3. Lam, Y. W., Lamond, A. I., Mann, M., and Andersen, J. S. (2007) Analysis of nucleolar protein dynamics reveals the nuclear degradation of ribosomal proteins. *Curr. Biol.* **17,** 749–760
4. Boisvert, F. M., Ahmad, Y., Gierlinski, M., Charriere, F., Lamond, D., Scott, M., Barton, G., and Lamond, A. I. (2011) A quantitative spatial proteomics analysis of proteome turnover in human cells. *Mol. Cell. Proteomics*, 10.1074/mcp.M111.011429
5. Schwanhäusser, B., Busse, D., Li, N., Dittmar, G., Schuchhardt, J., Wolf, J., Chen, W., and Selbach, M. (2011) Global quantification of mammalian gene expression control. *Nature* **473,** 337–342
6. Hori, T., Osaka, F., Chiba, T., Miyamoto, C., Okabayashi, K., Shimbara, N., Kato, S., and Tanaka, K. (1999) Covalent modification of all members of human cullin family proteins by NEDD8. *Oncogene* **18,** 6829–6834
7. Pan, Z. Q., Kentsis, A., Dias, D. C., Yamoah, K., and Wu, K. (2004) Nedd8 on cullin: Building an expressway to protein destruction. *Oncogene* **23,** 1985–1997
8. Osaka, F., Kawasaki, H., Aida, N., Saeki, M., Chiba, T., Kawashima, S., Tanaka, K., and Kato, S. (1998) A new NEDD8-ligating system for cullin-4A. *Gene Dev.* **12,** 2263–2268
9. Huang, D. T., Ayrault, O., Hunt, H. W., Taherbhoy, A. M., Duda, D. M., Scott, D. C., Borg, L. A., Neale, G., Murray, P. J., Roussel, M. F., and Schulman, B. A. (2009) E2-RING expansion of the NEDD8 cascade confers specificity to cullin modification. *Mol. Cell* **33,** 483–495
10. Lyapina, S., Cope, G., Shevchenko, A., Serino, G., Tsuge, T., Zhou, C., Wolf, D. A., Wei, N., Shevchenko, A., and Deshaies, R. J. (2001) Promotion of NEDD8-CUL1 conjugate cleavage by COP9 signalosome. *Science* **292,** 1382–1385
11. Read, M. A., Brownell, J. E., Gladysheva, T. B., Hottelet, M., Parent, L. A., Coggins, M. B., Pierce, J. W., Podust, V. N., Luo, R. S., Chau, V., and Palombella, V. J. (2000) Nedd8 modification of Cul-1 activates SCF beta(TrCp)-dependent ubiquitination of I kappa B alpha. *Mol. Cell. Biol.* **20,** 2326–2333
12. Soucy, T. A., Smith, P. G., Milhollen, M. A., Berger, A. J., Gavin, J. M., Adhikari, S., Brownell, J. E., Burke, K. E., Cardin, D. P., Critchley, S., Cullis, C. A., Doucette, A., Garnsey, J. J., Gaulin, J. L., Gershman, R. E., Lublinsky, A. R., McDonald, A., Mizutani, H., Narayanan, U., Olhava, E. J., Peluso, S., Rezaei, M., Sintchak, M. D., Talreja, T., Thomas, M. P., Traore, T., Vyskocil, S., Weatherhead, G. S., Yu, J., Zhang, J., Dick, L. R., Claiborne, C. F., Rolfe, M., Bolen, J. B., and Langston, S. P. (2009) An inhibitor of NEDD8-activating enzyme as a new approach to treat cancer. *Nature* **458,** 732–736
13. Jia, L., Li, H., and Sun, Y. (2011) Induction of p21-dependent senescence by an NAE inhibitor, MLN4924, as a mechanism of growth suppression. *Neoplasia* **13,** 561–569
14. Liao, H., Liu, X. J., Blank, J. L., Bouck, D. C., Bernard, H., Garcia, K., and Lightcap, E. S. (2011) Quantitative proteomic analysis of cellular protein modulation upon inhibition of the NEDD8-activating enzyme by MLN4924. *Mol. Cell. Proteomics*, 10.1074/mcp.M111.009183

15. Doyon, Y., and Côté, J. (2004) The highly conserved and multifunctional NuA4 HAT complex. *Curr. Opin. Genet. Dev.* **14,** 147–154
16. Zhang, P., Du, J., Sun, B., Dong, X., Xu, G., Zhou, J., Huang, Q., Liu, Q., Hao, Q., and Ding, J. (2006) Structure of human MRG15 chromo domain and its binding to Lys36-methylated histone H3. *Nucleic Acids Res.* **34,** 6621–6628
17. Pardo, P. S., Leung, J. K., Lucchesi, J. C., and Pereira-Smith, O. M. (2002) MRG15, a novel chromodomain protein, is present in two distinct multiprotein complexes involved in transcriptional activation. *J. Biol. Chem.* **277,** 50860–50866
18. Leung, J. K., Berube, N., Venable, S., Ahmed, S., Timchenko, N., and Pereira-Smith, O. M. (2001) MRG15 activates the B-myb promoter through formation of a nuclear complex with the retinoblastoma protein and the novel protein PAM14. *J. Biol. Chem.* **276,** 39171–39178
19. Beckett, D. (2004) Functional switches in transcription regulation: Molecular mimicry and plasticity in protein-protein interactions. *Biochemistry* **43,** 7983–7991
20. Zhang, P., Zhao, J., Wang, B., Du, J., Lu, Y., Chen, J., and Ding, J. (2006) The MRG domain of human MRG15 uses a shallow hydrophobic pocket to interact with the N-terminal region of PAM14. *Protein Sci* **15,** 2423–2434
21. Tominaga, K., Magee, D. M., Matzuk, M. M., and Pereira-Smith, O. M. (2004) PAM14, a novel MRG- and Rb-associated protein, is not required for development and T-cell function in mice. *Mol. Cell. Biol.* **24,** 8366–8373
22. Torres, J. Z., Miller, J. J., and Jackson, P. K. (2009) High-throughput generation of tagged stable cell lines for proteomic analysis. *Proteomics* **9,** 2888–2891
23. Boulon, S., Pradet-Balade, B., Verheggen, C., Molle, D., Boireau, S., Georgieva, M., Azzag, K., Robert, M. C., Ahmad, Y., Neel, H., Lamond, A. I., and Bertrand, E. (2010) HSP90 and its R2TP/prefoldin-like cochaperone are involved in the cytoplasmic assembly of RNA polymerase II. *Mol. Cell* **39,** 912–924
24. Boisvert, F. M., Lam, Y. W., Lamont, D., and Lamond, A. I. (2010) A quantitative proteomics analysis of subcellular proteome localization and changes induced by DNA damage. *Mol. Cell. Proteomics* **9,** 457–470
25. Wessel, D., and Flügge, U. I. (1984) A method for the quantitative recovery of protein in dilute solution in the presence of detergents and lipids. *Anal. Biochem.* **138,** 141–143
26. Bereman, M. S., Egertson, J. D., and MacCoss, M. J. (2011) Comparison between procedures using SDS for shotgun proteomic analyses of complex samples. *Proteomics* **11,** 2931–2935
27. Haas, W., Faherty, B. K., Gerber, S. A., Elias, J. E., Beausoleil, S. A., Bakalarski, C. E., Li, X., Villén, J., and Gygi, S. P. (2006) Optimization and use of peptide mass measurement accuracy in shotgun proteomics. *Mol. Cell. Proteomics* **5,** 1326–1337
28. Cox, J., and Mann, M. (2008) MaxQuant enables high peptide identification rates, individualized p.p.b.-range mass accuracies and proteome-wide protein quantification. *Nat. Biotechnol.* **26,** 1367–1372
29. Szymczak, A. L., Workman, C. J., Wang, Y., Vignali, K. M., Dilioglou, S., Vanin, E. F., and Vignali, D. A. (2004) Correction of multi-gene deficiency in vivo using a single "self-cleaving " 2A peptide-based retroviral vector. *Nat. Biotechnol.* **22,** 589–594
30. Sy, S. M., Huen, M. S., and Chen, J. (2009) MRG15 is a novel PALB2-interacting factor involved in homologous recombination. *J. Biol. Chem.* **284,** 21127–21131
31. Hayakawa, T., Zhang, F., Hayakawa, N., Ohtani, Y., Shinmyozu, K., Nakayama, J., and Andreassen, P. R. (2010) MRG15 binds directly to PALB2 and stimulates homology-directed repair of chromosomal breaks. *J. Cell Sci.* **123,** 1124–1130
32. Bengtsson, L., and Otto, H. (2008) LUMA interacts with emerin and influences its distribution at the inner nuclear membrane. *J. Cell Sci.* **121,** 536–548
33. Uhlen, M., Oksvold, P., Fagerberg, L., Lundberg, E., Jonasson, K., Forsberg, M., Zwahlen, M., Kampf, C., Wester, K., Hober, S., Wernerus, H., Björling, L., and Ponten, F. (2010) Towards a knowledge-based Human Protein Atlas. *Nat. Biotechnol* **28,** 1248–1250
34. Jackson, S., and Xiong, Y. (2009) CRL4s: The CUL4-RING E3 ubiquitin ligases. *Trends Biochem. Sci* **34,** 562–570
35. Christensen, M. E., and Dixon, G. H. (1982) Hyperacetylation of histone-H4 correlates with the terminal, transcriptionally inactive stages of spermatogenesis in rainbow trout. *Dev. Biol.* **93,** 404–415
36. Govin, J., Caron, C., Lestrat, C., Rousseaux, S., and Khochbin, S. (2004) The role of histones in chromatin remodelling during mammalian spermiogenesis. *Eur. J. Biochem.* **271,** 3459–3469
37. Auger, A., Galarneau, L., Altaf, M., Nourani, A., Doyon, Y., Utley, R. T., Cronier, D., Allard, S., and Côté, J. (2008) Eaf1 is the platform for NuA4 molecular assembly that evolutionarily links chromatin acetylation to ATP-dependent exchange of histone H2A variants. *Mol. Cell. Biol.* **28,** 2257–2270
38. Kelley, L. A., and Sternberg, M. J. (2009) Protein structure prediction on the Web: A case study using the Phyre server. *Nat. Protoc* **4,** 363–371
39. Thompson, J. D., Higgins, D. G., and Gibson, T. J. (1994) Clustal-W: Improving the sensitivity of progressive multiple sequence alignment through sequence weighting, position-specific gap penalties and weight matrix choice. *Nucleic Acids Res.* **22,** 4673–4680
40. Waterhouse, A. M., Procter, J. B., Martin, D. M., Clamp, M., and Barton, G. J. (2009) Jalview version 2: A multiple sequence alignment editor and analysis workbench. *Bioinformatics* **25,** 1189–1191